Driving nuclei with resonant electrons: *Ab initio* study of $(e+H_2)\,^2\Sigma_u^+$

F. Robicheaux*
Department of Physics and The James Franck Institute, University of Chicago, Chicago, Illinois 60637
(Received 21 November 1990)

We have calculated the cross sections for vibrational excitation and dissociative attachment in H_2 below 5 eV scattering energy. This completely *ab initio* calculation uses the frame-transformation method of Greene and Jungen [Adv. At. Mol. Phys. **21**, 51 (1985)] for electron-vibronic coupling in resonant scattering from a neutral molecule. We found it necessary to modify their method to obtain good agreement with previous theory and experiment for $v=0\rightarrow v_f$ with $v_f=1-3$; for larger v_f and for dissociative attachment we obtained good agreement with previous theory and qualitative agreement with experiment. The fixed-nuclei phase shifts were derived from a fully *ab initio* calculation in prolate spheroidal coordinates and then transformed to spherical $l=1$ phase shifts. The vibrational structure of H_2^- becomes evident for excitation from higher vibrational states of H_2 as well as for larger Δv's, confirming previous theory and experiment.

I. INTRODUCTION

This paper concentrates on the vibrationally inelastic processes in electron-H_2 scattering below 5 eV, measured from the $H_2(v=0,J=0)$ state, as a specific example of electron-molecule scattering.[1-3] Under these restrictions, the $^2\Sigma_u^+$ resonance at 3 eV is the only state which contributes. The next resonance, $^2\Sigma_g^+$ at 10 eV above the ground state, does not contribute to the cross section in our energy range. Nonresonant processes contribute very little due to the small electron-to-nuclear mass ratio. The polarizability of the neutral molecule is very small due to its completely filled electronic shell, and its lowest multipole moment is a small quadrupole term, so that the electron "feels" only a very small long-range force.

At an internuclear distance of 3 a.u. the resonance becomes a true bound state, H^-+H. If the resonant electron has enough energy and remains attached long enough, it can break the H_2 bond and stick to one of the atoms, dissociative attachment.[4] This extreme case of "vibronic excitation" will be considered on the same footing as the more usual vibrational excitation. Lastly, three quarters of a volt above the dissociation attachment threshold, the triple breakup $(e+H+H)$ channel opens. However, this process is very unlikely below 9 eV, the energy needed to excite the repulsive $^3\Sigma_u^+$ electronic state of H_2 at its equilibrium distance.

The theoretical approach to inelastic processes in electron-molecule scattering has been dominated by two complementary, rather accurate, methods. The complex potential method[5] (resonance theory) centers on the motion of the negative ion during a resonance lifetime. The nuclei move on a complex potential, its real part being the energy and its imaginary part being the width of the resonance. The width decreases with increased internuclear distance R owing to the increased size of the resulting potential well *and* to the evolution of closed molecular shells toward open atomic shells. In the $H_2^-\,^2\Sigma_u^+$ resonance, the width *vanishes* for $R>3$ a.u. indicating a true bound state. Alternatively, the frame-transformation method[6] matches phase shifts of the electron at each internuclear distance onto phase shifts and couplings of rovibrational states of the neutral molecule. It assumes the Born-Oppenheimer approximation holds while the electron is near the nuclei. A resonance manifests itself as a rapid variation of the phase shift with electronic energy at each R. Both methods can be used for model problems or for fitted potentials (e.g., $e+N_2$).[7,8] However, the local complex potential method does not seem to be as well suited to *ab initio* calculations,[9] especially if the resonance width is large (a nonlocal complex potential method increases the accuracy but with a decrease in clarity[10]); it is inherently limited by its initial approximation, while the frame-transformation method is in principle exact and can be made more precise with increased effort. On the other hand, the energy and lifetime concepts of the complex potential method are more easily transferred to features of the cross section.

This paper will use the theoretical formulation of Greene and Jungen (similar to that of Schneider and coworkers[11]) as the basis for the transfer of body-frame, fixed-nuclei information to laboratory-frame scattering parameters. This framework has been successfully applied to photoionization and dissociation of molecules[12] and to fitted electron-molecule scattering,[6,8] but has not been applied previously to *ab initio* electron–neutral-species processes. We found that a modified version of the Greene-Jungen (GJ) program, as spelled out in their "boomerang-type" calculation[8] of $e+N_2$, worked well for low Δv (<3) but exhibited anomalies for the larger Δv's (>3) or for dissociative attachment, both of which have very small cross sections. The difficulties of the GJ program and its slight modification are described in Secs. III A and III B.

A main reason for focusing on $e+H_2$ scattering is that there are only three electrons so that a completely *ab initio* calculation of fixed-nuclei phase shifts is not impossi-

ble but is still interesting. The frame-transformation method requires the fixed-nuclei phase shift of the scattering electron for each of the relevant channels and the coupling between channels. None of the electronically excited states can be reached in the <5 eV energy range at the equilibrium distance of H_2. This leaves only the different angular momentum states of the scattering electron as possible channels. Of these, only the $p\sigma$ wave through the $^2\Sigma_u^+$ resonance in the body frame contributes to the *inelastic* cross section. The Greene-Jungen program is, of course, able to handle more than one channel, but the reduction to a single-channel problem facilitates the assessment of its strengths when applied to electron–neutral-species scattering.

By far the most time-consuming part of the calculation lies in computing the fixed-nuclei phase shift of the electron as a function of electronic energy. This was accomplished by an R-matrix calculation in prolate spheroidal coordinates which gave the *phase* of the wave function at the surface of a spheroidal box. Remember that the R-matrix calculation does not depend at all on the outside boundary conditions of the wave function (e.g., for channels with negative kinetic energy at infinity, convergence or divergence of the wave function has no effect on the R-matrix calculation). Multichannel quantum-defect technology (MQDT) treats the wave function outside of the box.[13]

The regular and irregular radial prolate spheroidal waves[14] are superposed to match the R matrix calculated on the surface of the box. These phase-shifted spheroidal waves were then transformed to phase-shifted spherical waves to obtain the fixed-nuclei scattering parameters. At this point a comparison of the phase of the p and f waves showed the dominance of the $l=1$ channel. We did not try to calculate in spherical coordinates directly feeling unable to accurately produce H^-+H properties at large internuclear distances, $R>3$ a.u. Evolution of the doublet nature of the electronic state, which evolves from a singlet H_2 plus electron at small R to a singlet H^- plus H atom at large R, is essential to this process.

The rotational coupling yields mainly a transformation of Hund's case b states (relevant at small r) to Hund's case d (large r), which will not be discussed in detail as it is well understood.[6] The long-range polarization and multipole fields also induce a rotational coupling which could be handled in an MQDT formulation[13] which is independent of the short-range dynamics.

II. FIXED-NUCLEI PHASE SHIFTS

A. R matrix in spheroidal coordinates

The electronic part of the calculation was performed in prolate spheroidal coordinates. These are

$$\xi=\frac{r_1+r_2}{R},\quad \eta=\frac{r_1-r_2}{R} \tag{1}$$

(where r_i is the distance from the electron to nucleus i) and the angle of rotation φ about the internuclear axis. The internuclear distance R is fixed in this part. The metric in this coordinate system is

$$h_\xi=\frac{R}{2}\left[\frac{\xi^2-\eta^2}{\xi^2-1}\right]^{1/2},$$
$$h_\eta=\frac{R}{2}\left[\frac{\xi^2-\eta^2}{1-\eta^2}\right]^{1/2}, \tag{2}$$
$$h_\varphi=\frac{R}{2}[(\xi^2-1)(1-\eta^2)]^{1/2}.$$

It is well known that the electronic motion in H_2^+ separates in this system.[15] The accurate electronic states of H_2 are also calculated in this coordinate system.[16]

In the usual R-matrix formulation, the normal logarithmic derivative of the wave function is assumed constant over a closed surface specified by fixing one of the coordinates of an orthogonal system,[17]

$$\frac{1}{h_1}\frac{\partial\Psi}{\partial x_1}+b\Psi=0,\quad x_1=\text{const}. \tag{3}$$

In our case, the surface is defined by $\xi=\xi_c=$const. This definition of b (the negative of the normal logarithmic derivative) leads to complications in prolate spheroidal coordinates not encountered in spherical coordinates where $h_r=1$ everywhere. One thus needs to examine the variational principle for b.

The variational principle for b deals with the expression

$$b\int_S dS\,\Psi_t^2=2\int_v dV\,\Psi_t(E-H)\Psi_t-\int_S dS\,\Psi_t\frac{1}{h_\xi}\frac{\partial\Psi_t}{\partial\xi}, \tag{4}$$

with the surface defined by $\xi=\xi_c=$const. If Ψ_t is a trial wave function close to the real wave function Ψ at energy E, e.g., $\Psi_t=\Psi+\delta$, this equation gives b correctly to order δ^2. Notice how the left-hand side of this equation contains a weighting factor which has η^2 under a square root $(\xi_c^2-\eta^2)^{1/2}$, while the last term on the right does not due to the h_ξ in the denominator. This weighting factor can be removed by redefining b through

$$\frac{\partial\Psi}{\partial\xi}+b\Psi=0,\quad \xi=\xi_c. \tag{5}$$

The left-hand side of Eq. (4) transforms to

$$b\int_S dS\,\Psi_t^2\rightarrow b\int_S dS\frac{1}{h_\xi}\Psi_t^2. \tag{6}$$

This trivial change in definition leads to a large practical result. The first formulation does not ensure a symmetric K matrix (reaction matrix) if more than one spheroidal partial wave participates in the collision, while the second formulation does, thus eliminating unnecessary work. The two methods are equivalent in spherical coordinates where the R-matrix method is mostly used. The asymmetry of the K matrix is due to the lack of orthogonality of the angular harmonics over the surface. As a general rule of thumb, to obtain a symmetric K matrix the constant b in Eq. (3) should be replaced by $bw(\Omega)$ where w is a weighting function dependent on the angular coordinates $\Omega\equiv x_2,x_3,\ldots,x_n$ ($n-1$ is the dimensionality of

the surface). The weighting function must satisfy

$$\int_S d\Omega\, \phi_\lambda^* w \phi_\alpha = \delta_{\lambda\alpha} ,$$

where ϕ_λ are the angular harmonics. For a spherical surface in three dimensions $w=1$; for our case $w=1/h_\xi|_{\xi=\xi_c}$.

Wave functions were constructed from a basis of single-particle functions of the form

$$\psi_{nlm} = (\xi^2-1)^{|m|/2}\xi^n e^{-\beta\xi} P_{lm}(\eta) e^{im\varphi} . \quad (7)$$

They were then fully antisymmetrized to Fermi statistics and coupled to ${}^2\Sigma_u^+$ symmetry. The number of resulting basis functions grows very rapidly with the number of single-particle functions so that the calculation would quickly become unmanageable. The actual basis functions were thus limited to the following three types: (1) ${}^2\Sigma_u^+(X\,{}^1\Sigma_g^+ 1s\sigma^2 + p\sigma, f\sigma)$, i.e., the electronic ground state of H_2 plus single-particle functions of p and $f\sigma$ type. (2) ${}^2\Sigma_u^+(E,F\,{}^1\Sigma_g^+(1s\sigma 2s\sigma + 2p\sigma^2) + p\sigma)$; i.e., the first ${}^1\Sigma_g^+$ excited state plus single-particle functions of $p\sigma$ type. (3) ${}^2\Sigma_u^+$ (H^- $1s^2 + H$ $1s$); the Heitler-London $H^- + H$ wave function. A few other diffuse ${}^2\Sigma_u^+$ wave functions were added for insurance.

Previous workers[18] found that limiting the wave function to type (1) led to inelastic cross sections too small by $\sim 30\%$. The other two types are necessary to account for the relaxation and polarization of the core by the third electron while close to the core. Specifically, type (2) basis functions help account for relaxation of the core at small internuclear distances; including higher excited states of the core did not improve convergence. At large internuclear distances type (3) basis functions accounted for polarization effects. We were not able to bind the third electron at $R>3$ a.u. without the type (3) basis functions; our three electron bound-state energies were 50–100 meV higher than previous results.[19] The R-matrix "box" was large enough to be able to ignore polarization and multipole effects outside of it for the vibrationally inelastic scattering. The polarization potential outside of the box greatly affects the elastic channel, especially modifying the threshold behavior of the elastic cross section.

Figure 1 shows the fraction f of the wave function of type (1) at the "resonance energy" compared to type (3). This is necessarily a qualitative parameter as the type (1) and (3) wave functions are not orthogonal, and also the resonance energy is not well defined. This figure also describes the evolution of the wave function from the singlet coupling to H_2 to the singlet coupling of H^-. Note, especially the rapid drop of f between 2 and 3 a.u.

B. Fixed-nuclei scattering parameters

Outside of the R-matrix box at each fixed nuclear distance, the wave function is a superposition of a small number of spheroidal waves. These functions are solutions to Schrödinger's equation in prolate spheroidal coordinates with a constant potential, standard functions described in the usual references.[14] We transform the *phases* of the wave-function at the surface of the box into

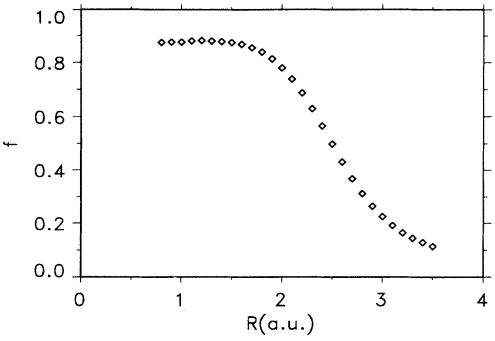

FIG. 1. Fraction f of the ${}^2\Sigma_u^+$ wave function coupled to singlet H_2 plus $p\sigma$ as a function of internuclear distance R.

phase-shifted standard functions outside, following the usual MQDT procedures.[13]

MQDT is designed to take advantage of the fact that once the electron is outside of the core it experiences a simple long-range field. At any energy there are two independent solutions of the radial Schrödinger equation, one of which converges at the origin while the other diverges (both of which we choose to be real). Outside the reaction surface at $\xi=\xi_c$, the wave function for an N-channel problem is

$$\Psi'_\lambda = \mathcal{A} \sum_{\lambda=1}^{N} \Phi_\lambda(\Omega;R)[f_{\varepsilon\lambda}(\xi)\delta_{\lambda\lambda'} - g_{\varepsilon\lambda}(\xi)K_{\lambda\lambda'}], \quad \xi>\xi_c \quad (8)$$

[Eq. (10) of Ref. 6(a)] where $\mathcal{A}$ is the antisymmetrization operator and $\Phi_\lambda(\Omega;R)$ is the electronic ground state of H_2 times the angular function of the third electron [$\Phi_\lambda = \psi_{H_2}\phi_{\lambda m}(\eta,\varphi)$]. In all that follows, $\mathcal{A}$ and ψ_{H_2} are implied but have no effect because ψ_{H_2} vanishes outside of the R-matrix box; they will not be written explicitly again. The functions $f_{\varepsilon\lambda}$ and $g_{\varepsilon\lambda}$ are the regular and irregular spheroidal waves of energy ε and $\phi_{\lambda m}(\eta,\varphi)$ is the prolate spheroidal harmonic, a standard function whose properties are well understood.[14]

The R-matrix specifies the wave function at the surface $\xi=\xi_c$ in the form

$$\Psi'_\lambda = -\sum_\lambda \frac{\partial\Psi_\lambda}{\partial\xi} R_{\lambda\lambda'} , \quad (9)$$

where $\mathbf{R}$ is a real, symmetric matrix. Simple substitution connects the K matrix to the R matrix

$$\mathbf{K} = \left[\mathbf{R}\frac{\partial\mathbf{g}}{\partial\xi} + \mathbf{g}\right]^{-1}\left[\mathbf{R}\frac{\partial\mathbf{f}}{\partial\xi} + \mathbf{f}\right] \quad (10)$$

[Eq. (3.20) of Ref. 6(c)] where for example $\mathbf{f}$ is a diagonal matrix whose λth element is $f_{\varepsilon\lambda}(\xi_c)$. The reaction matrix $\mathbf{K}$ is itself real and symmetric. Notice how the superposition, Eq. (8), holds whether or not the λth channel is open. Any divergences in closed channels are eliminated in a later step by superposing the Ψ_λ as necessary to

obtain convergence at infinity. By waiting to apply the boundary conditions at $\xi \to \infty$ we keep $\mathbf{K}$ free of unnecessary energy dependences. The arctangents of the eigenvalues of $\mathbf{K}$ are the phase shifts.

The fixed-nuclei phase shifts were calculated on a mesh in R of size 0.1 a.u., with an energy mesh of 10^{-3} a.u. at each R. The size of the R-matrix box varied with internuclear separation R to reflect the scaling of ξ. The size of the box should be large enough to include all of the complicated dynamics near the core without wasting effort recalculating standard functions. Instead of changing ξ_c continuously as R increases, I kept it fixed over each of four different ranges: $\xi_c=9$; $0.7 < R < 1.0$; $\xi_c=8$; $1.1 < R < 1.8$; $\xi_c=7$; $1.9 < R < 2.6$; $\xi_c=6$; $2.7 < R < 3.5$. Notice how one of the ranges covers the ground vibrational state to minimize the effects of any possible "kinks" between the different ranges. Over 99% of the total calculation time was spent on the procedures described in this section.

C. Transformation to spherical coordinates

Up to this point, the wave function outside of the box involves a superposition of spheroidal waves. The prolate spheroidal coordinates depend explicitly on the internuclear distance R, a feature incompatible with treatment of the different vibrational states. This necessitates a transformation from spheroidal to spherical waves. The fixed-nuclei calculation included only p and f spheroidal waves. The reaction matrix (K matrix) is symmetric in prolate spheroidal coordinates, but the corresponding K matrix in spherical coordinates is not necessarily symmetric due to the truncation to two partial waves. The amount of asymmetry places a lower limit on the convergence of the calculation.

The wave function outside of the box is

$$\Psi_{e\lambda'}=\sum_{\lambda}\phi_{\lambda 0}(\eta,\varphi;\varepsilon;R)[f_{\varepsilon\lambda}(\xi;R)\delta_{\lambda\lambda'}-g_{\varepsilon\lambda}(\xi;R)K_{\lambda\lambda'}]$$
$$=\sum_{l} Y_{l0}(\theta;\varphi)[f_{\varepsilon l}(r)I_{l\lambda'}-g_{\varepsilon l}(r)J_{l\lambda'}] , \quad (11)$$

where $\phi_{\lambda 0}$ is the $(\lambda, m=0)$ spheroidal harmonic, $f_{\varepsilon\lambda}$ ($g_{\varepsilon\lambda}$) is the regular (irregular) spheroidal wave of energy ε, $f_{\varepsilon l}$ ($g_{\varepsilon l}$) is the regular (irregular) spherical Bessel function, with l and λ are restricted to the values 1 and 3. These two superpositions hold everywhere outside of the R-matrix box so we can choose any convenient radius for the transformation. Remember that the $K_{\lambda\lambda'}$ were found at an earlier step of the calculation, Eq. (10).

Of course, the most convenient place for the matching is at $r \to \infty$, where

$$\xi \to \frac{2r}{R}, \quad \eta \to \cos\theta, \quad \varphi \to \varphi . \quad (12)$$

The asymptotic form of $f_{\varepsilon\lambda}$ ($g_{\varepsilon\lambda}$) becomes the same (within a sign) as $f_{\varepsilon l}$ ($g_{\varepsilon l}$). We can now read off **I** and **J**

$$I_{l\lambda'}=\langle Y_{l0}|\phi_{\lambda' 0}\rangle ,$$
$$J_{l\lambda'}=\sum_{\lambda}\left[\lim_{r\to\infty}\frac{g_{\varepsilon\lambda}(2r/R;R)}{g_{\varepsilon l}(r)}\right]\langle Y_{l0}|\phi_{\lambda 0}\rangle K_{\lambda\lambda'} . \quad (13)$$

The K matrix in spherical coordinates is simply $\mathbf{K}=\mathbf{J}\mathbf{I}^{-1}$.

The largest coupling to the f wave and the largest asymmetries of the K matrix occur at the largest internuclear distance (in this case 3.5 a.u.). The maximum asymmetry is 1% of the off-diagonal elements, and the f-wave phase shift is less than 0.02 at this R; we need only retain $K_{11}=\tan\pi\mu$ for accurate cross sections. The phase shift $\pi\mu$ depends on the electronic energy and on the internuclear distance; it contains all of the information about the interaction of the electron with the core.

Some of the energy dependence of the p-wave phase shift is due to threshold effects of short-range potentials. We remove this trivial dependence by defining[13]

$$\tan\pi\mu_0(\varepsilon;R)=|k|^{-2l-1}\tan\pi\mu(\varepsilon;R) , \quad (14)$$

where the angular momentum l is unity for our case. The μ_0 has a much smaller energy dependence, even for resonances near threshold. Figure 2 shows μ_0 as a function of energy above the H_2 potential curve at $R=1$, 2, and 3 a.u. An important feature to note is that none of the values of μ_0 (ε;1 a.u.) plotted in Fig. 1 equals any of the values of $\mu_0(\varepsilon';3$ a.u.) [i.e., it is impossible to draw a horizontal line on Fig. 1 which intersects the two curves $\mu_0(\varepsilon;1$ a.u.) and $\mu_0(\varepsilon;3$ a.u.)]; the transcendental equation $\mu_0(V^{\tau}(R);R)=\tau$ does not have a solution for all values of R. The phenomenological model employed by Greene and Jungen[8] did not have this property.

At an internuclear spacing of 1.4 a.u., our value of μ_0 was practically constant with energy: $\mu_0(\varepsilon,1.4)=0.44$. The μ_0 obtained from the phase shift of Ref. 15(b) decreased nearly linearly from 0.43 at $\varepsilon=0$ to 0.40 at $\varepsilon=0.18$ a.u. above the ground electronic state of H_2. For comparison we define an equilibrium cross section to be $\sigma_{eq}=(4\pi/k^2)\sin^2\pi\mu$. The σ_{eq} derived from our data is nearly twice as large as the σ_{eq} found using the data of Ref. 15(b). This is not altogether surprising since their calculation utilized a frozen electronic core. Our σ_{eq} was also not in very good agreement with that of Gibson and Morrison.[20] Their $\sigma_{eq}\sim 0.3$ a.u. at threshold and peaked at $\sim$20 a.u. near 4.5 eV, whereas our $\sigma_{eq}=0$ at threshold and peaked at $\sim$20 a.u. near 5.5 eV. The discrepancy near threshold is due to our ignoring multipole fields and

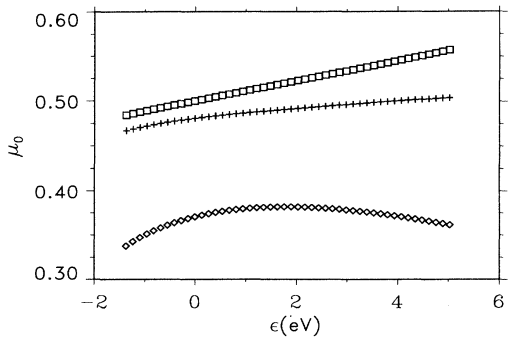

FIG. 2. "Energy independent" quantum defect μ_0 as a function of electron energy ε for the internuclear distances: $R=1$ a.u. (◇), 2 a.u. (+), and 3 a.u. (□).

polarizability outside of the R-matrix box. We do not expect our approximations to work very well for elastic scattering.

III. FRAME TRANSFORMATION

A. Greene-Jungen method and its difficulties

The basic idea behind the frame transformation rests on the division of space into a reaction zone and an outside region. Inside of the reaction zone, the good quantum numbers for the electron are the internuclear distance R and the electronic energy ε. Outside of the reaction zone, the good quantum numbers are the electron's kinetic energy and the vibrational state v of the molecule. The two regions are connected by a simple projection on the boundary.

The Greene-Jungen program as expressed in their N_2 paper takes the following form.[8] After calculating the fixed-nuclei phase shifts, you remove the main energy dependence by factoring out the trivial threshold effects. For example, you select the nearly energy independent quantum defect for pure-l-wave scattering given by Eq. (14). In the next step, you define a potential curve $V^\tau(R)$ by solving the transcendental equation $\mu_0(V^\tau(R);R)=\tau$ and add it to the original H_2 potential curve, $V^{H_2}(R)$. $V^\tau(R)$ is the additional potential "felt" by the nuclei due to the third electron. Although this is one of the more trivial steps and is very easy to implement for their model problem, a quick glance at Fig. 2 shows this step to be impossible in practice as noted above. For example, the horizontal line $\tau=0.3$ would intersect μ_0 for $R=3$ a.u. at an unrealistic energy (similarly the line $\tau=0.5$ does not intersect μ_0 for $R=1$ a.u. in our energy range). This result was unexpected by us even though implied by previously published phase shifts for $e+H_2$,[21] and is due to the nonresonant behavior at small R. We would not expect the same problem for $e+N_2$ scattering which has a much sharper resonance.

We adapted the GJ program by changing its focus from μ_0 to the phase ζ of the wave function defined by[6(c)]

$$\tan\pi\zeta(\varepsilon;R)=-\frac{\partial}{\partial r}\ln\Psi_\varepsilon(r;R)\bigg|_{r=r_c} . \tag{15}$$

Figure 3 shows $\zeta(\varepsilon;R)$ for $R=1$, 2, and 3 a.u. Notice how the resonance sharpens and drops in energy as R increases. Also, ζ is monotonic with energy and covers roughly the same range for different values of R. For these reasons, we can define the added potential curve $V^\tau(R)$ by setting $\zeta(V^\tau(R);R)=\tau$. Figure 4 shows $V^{\tau=0.5}(R)$, which is repulsive over the whole range shown. We next calculate the vibrational eigenstates $\chi_v^\tau(R)$ and energies ε_v^τ for the combined potential $V^{H_2}(R)+V^\tau(R)$, where $V^{H_2}(R)$ is the vibrational potential of the H_2 molecule. Finally, τ is varied until one of the ε_v^τ matches the total energy, E. When the ε_v^τ coincides with E, we know that the wave function at the surface $r=r_c$ has the form

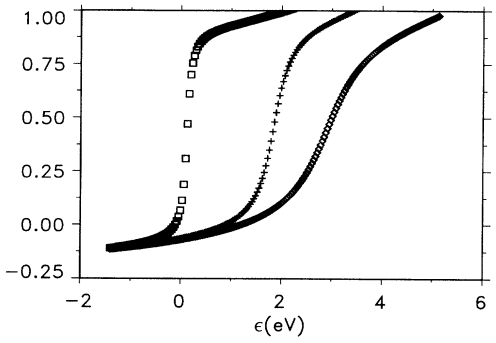

FIG. 3. Phase ζ of the electronic part of the wave function vs ε at $r=9$ a.u. for the internuclear distances: $R=1$ a.u. ($\diamond$), 2 a.u. ($+$), and 3 a.u. ($\square$).

$$\Psi_{Ev}=N^\tau(R)\chi_v^\tau(R)\cos\pi\tau ,$$
$$\frac{\partial\Psi_{Ev}}{\partial r}=-N^\tau(R)\chi_v^\tau(R)\sin\pi\tau . \tag{16}$$

Here

$$N^\tau(R)=\left[\frac{\partial\zeta(\varepsilon;R)}{\partial\varepsilon}\right]^{-1/2} \tag{17}$$

normalizes Ψ_{Ev} at each R through keeping the volume integral of the electronic part of the wave function independent of R.[6(c)] These Ψ_{Ev} match the asymptotic solution of the full Schrödinger equation by projection onto the vibrational states of the H_2 molecule, $\chi_v(R)$,

$$\Psi_{Ev}(r_c,R)=\sum_{v'}\chi_{v'}(R)C_{v'v} ,$$
$$\frac{\partial\Psi_{Ev}(r_c,R)}{\partial r}=-\sum_{v'}\chi_{v'}(R)S_{v'v} , \tag{18}$$

where

$$C_{v'v}=\int dR\,\chi_{v'}^\tau(R)N^\tau(R)\chi_v^\tau(R)\cos\pi\tau \tag{19}$$

and $S_{v'v}$ is given by a similar equation.[6,8] The R matrix is simply $-\mathbf{CS}^{-1}$ and should be real and symmetric.

The reaction matrix $\mathbf{K}$ contains all of the scattering in-

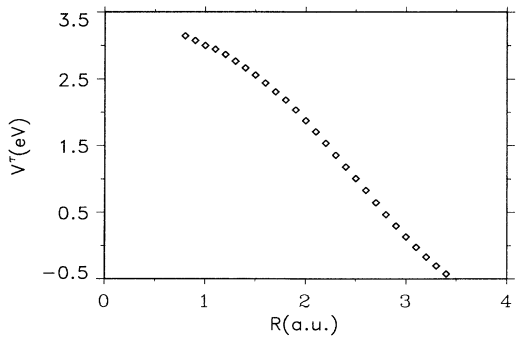

FIG. 4. Additional potential $V^\tau(R)$ for $\tau=0.5$ at $r=9$ a.u.

formation and is given by Eq. 10 where **f** and **g** (and their derivatives) are diagonal matrices whose vth elements are $f_{E-\varepsilon_v,l}(r_c)$ and $g_{E-\varepsilon_v,l}(r_c)$ (and their derivatives). In our case, the f and g are spherical Bessel functions with $l=1$, usually denoted j and y. We are ignoring the polarization and quadrupole potential outside of the R-matrix box; they only contribute to the rotational excitation and elastic cross sections.

Varying τ until one of the ε_v^τ matches the total energy E and recalculating $\chi_v^\tau(R)$ each time would be impractically slow. In practice, the ε_v^τ, **C**, and **S** are calculated at several different τ. The smallest mesh size we tried was $\delta\tau=0.02$. We then interpolate the parameters at each E. The symmetry of the R matrix tests the accuracy of the interpolation and of the whole calculation because we have done nothing which guarantees its symmetry. This procedure yielded asymmetries at the percent level. To complete the calculation, we artifically symmetrized the R matrix by setting $R_{ij}=\frac{1}{2}(R_{ij}+R_{ji})$ (artificially symmetrizing the K matrix produced essentially the same results). The cross sections for low Δv (<3) were fine. However, the high Δv (>3) cross sections were completely unrealistic; several normal points were followed by a discontinuous shift in the cross section by up to 30%. The dissociative attachment cross section also suffered from these anomalies. These anomalies, confined to $v\rightarrow v'$ cross sections smaller than the $v\rightarrow v+1$ by 2–3 orders of magnitude (the level of asymmetry in the R matrix), required further adaptation of the GJ method.

The anomalies might result from the rapid energy dependence of the phase, especially at large R, which decreases the accuracy of the interpolation; the Greene-Jungen program was devised with nearly energy-independent parameters in mind. The immediate source of the problem seems to lie in the *small* off-diagonal R-matrix elements. Artificially symmetrizing the R matrix essentially replaces the far off-diagonal elements with small random numbers. A scheme that guarantees the symmetry of the R matrix appears necessary.

B. Fine tuning the Greene-Jungen method

The solution to this problem lies in using a physically more relevant interpolation, namely, on the eigenchannel R matrix.[11,17] Instead of calculating the χ_v^τ and ε_v^τ for the ~ 50 different values of τ necessary to make a meaningful interpolation, we did so for only three different values of $\tau=\zeta(V^\tau(R);R)$: $0,\frac{1}{2},1$ (the electronic wave function with $\tau=1$ has one more node than the wave function with $\tau=0$). These wave functions served then as input for a variational calculation of the R matrix of the type described in the Appendix. In other words, we used exact eigenstates of the total Born-Oppenheimer Hamiltonian at the energies ε_v^τ as the basis functions of an eigenchannel R-matrix calculation. The eigenchannel R matrix interpolates nearly as accurately as the more laborious version described in Sec. III A, while ensuring its symmetry. This radical reduction of interpolation points yields accurate cross sections only for energies less than 5 eV above the H_2 ground state. We could increase this range by including higher values of τ.

The R-matrix box is defined as $r<r_c$ and $R<R_c$. The final results were insensitive to the box size. The cross section varied at the percent level for 7 a.u. $<r_c<10$ a.u. We chose $r_c=9$ a.u. and $R_c=3.5$ a.u. for the final calculations. The boundary condition for the total wave function on the surface of this box is $(\partial\Psi/\partial r)+b\Psi=0$ at $r=9$ a.u. and $(\partial\Psi/\partial R)+bM\Psi=0$ at $R_c=3.5$ a.u. where M is the nuclear reduced mass and m, the reduced mass of the electron, was taken to be 1 a.u.

The total wave functions used in this final R-matrix calculation are of a particularly simple type. One class sets $\tau=0$ for the electronic wave function. We then solve for the nuclear motion on the resulting potential curve such that the nuclear function equals zero at $R=R_c$. The total wave function for this class is then $\Psi_{\tau v}^T=\chi_v^\tau(R)\psi_{\rm el}^\tau(R;r)$ and has the total energy ε_v^τ. The second class sets $\tau=1$ for the electronic wave function. Again we set the nuclear function equal to zero at the boundary. Notice that the $\Psi_{\tau v}^T$ are orthonormal inside the R-matrix box and satisfy

$$\langle\Psi_{\tau v}^T|H|\Psi_{\tau' v'}^T\rangle=\varepsilon_v^\tau\delta_{\tau\tau'}\delta_{vv'}\ , \tag{20}$$

where the integration is over the space inside the box. The third class sets $\tau=0.5$ for the electronic function. Again we set the nuclear function equal to zero at the boundary; however, to this class we also add two nuclear functions whose *derivatives* are zero at $R=R_c=3.5$ a.u. Now the total basis set, including all three classes, is not orthogonal. In this basis

$$\Lambda_{\tau v,\tau' v'}=\cos\pi\tau\cos\pi\tau'\int_0^{R_c}dR\ N^\tau(R)\chi_v^\tau N^{\tau'}(R)\chi_{v'}^{\tau'}+\chi_v^\tau(R_c)\chi_{v'}^{\tau'}(R_c)\int_0^{r_c}dr\ \psi_{\rm el}^\tau(R_c;r)\psi_{\rm el}^{\tau'}(R_c;r) \tag{21}$$

and

$$\Gamma_{\tau v,\tau' v'}=2(E-\varepsilon_{v'}^{\tau'})\int_0^{R_c}dR\ \chi_v^\tau(R)\chi_{v'}^{\tau'}(R)\int_0^{9}dr\ \psi_{\rm el}^\tau(R;r)\psi_{\rm el}^{\tau'}(R;r)+\cos\pi\tau\sin\pi\tau'\int_0^{R_c}dR\ N^\tau(R)\chi_v^\tau(R)N^{\tau'}(R)\chi_{v'}^{\tau'}(R)$$

$$-\frac{1}{M}\left[\chi_v^\tau\frac{\partial\chi_{v'}^{\tau'}}{\partial R}\right]_{R_c}\int_0^{r_c}dr\ \psi_{\rm el}^\tau(R_c;r)\psi_{\rm el}^{\tau'}(R_c;r)\ . \tag{22}$$

Note, the integrals $\int_0^{r_c} dr\, \psi_{\rm el}^{\tau}(R;r)\psi_{\rm el}^{\tau'}(R;r)$ can be solved without resorting to actual integration by using the trick

$$\int_0^{x_f} dx(\psi_i H\psi_j - \psi_j H\psi_i) = (\varepsilon_j - \varepsilon_i)\int_0^{x_f} dx\, \psi_j\psi_i \ . \quad (23)$$

This equation holds if the ψ are eigenstates of the Hamiltonian, H. On the left-hand side of (23), the potential term cancels leaving only the kinetic energy. Thus the left-hand side of (23) can be reduced to

$$-\tfrac{1}{2}\int_0^{x_f} dx \frac{\partial}{\partial x}\left[\psi_i\frac{\partial\psi_j}{\partial x} - \psi_j\frac{\partial\psi_i}{\partial x}\right] .$$

The only necessary integrations in Eqs. (21) and (22) are over the internuclear coordinate R. In the actual calculation we assumed the Born-Oppenheimer approximation was exact. Because it is not exact, the resulting real matrix Γ is slightly asymmetric, which has been removed by symmetrizing the Γ calculated at this stage, i.e., $\Gamma_{\tau v,\tau' v'} = \frac{1}{2}(\Gamma_{\tau v,\tau' v'} + \Gamma_{\tau' v',\tau v})$. We then follow the procedure described in Appendix to get a variational estimate for the R matrix and convert it into the K matrix. The closed channels (i.e., channels with negative kinetic energy) are eliminated to obtain the final K matrix.

The dissociative attachment channel still evolves for $R > 3.5$ a.u. We assume this evolution is well described by an accurate adiabatic potential which we obtained from the literature.[19] We numerically integrated the Schrödinger equation inward from infinity. We then matched the resulting f and g to the R-matrix results at $R = 3.5$ a.u., Eq. (10). Note, for the dissociative attachment channel in Eq. (10)

$$\frac{\partial f}{\partial R}\left[\frac{\partial g}{\partial R}\right]$$

is replaced with

$$\frac{1}{M}\frac{\partial f}{\partial R}\left[\frac{1}{M}\frac{\partial g}{\partial R}\right] ,$$

where

$$\frac{\partial f}{\partial r}\left[\frac{\partial g}{\partial r}\right]$$

is equivalent to

$$\frac{1}{m}\frac{\partial f}{\partial r}\left[\frac{1}{m}\frac{\partial g}{\partial r}\right] .$$

For energies less than 3.7 eV, the dissociative attachment channel is closed, which is the source of the resonance structure in Figs. 5 and 6.

Of the cross sections shown in this paper, the refinement of the GJ method presented in this section only affects the dissociative attachment cross section to a visible extent. However, the computation of cross sections using the method described in Sec. III A was an order of magnitude slower than the computation described in this section. This is due to the change in the number of potential curves for which we needed to calculate vibrational functions. Both of these times were insignificant compared to the time needed to calculate the fixed-nuclei phase shifts. All of the calculations were performed on a Silicon Graphics 4D/240 which is ~3.7 megaflops per processor (~2 times faster than the DECstation 3100). The fixed-nuclei phase shifts required ~2 CPU h, while the calculations described in Sec. III A (III B) took ~2 CPU min (~15 CPU sec).

IV. RESULTS

We have calculated integral cross sections for vibrational excitation and for dissociative attachment from molecules in the $v = 0$–2 vibrational states. We examined

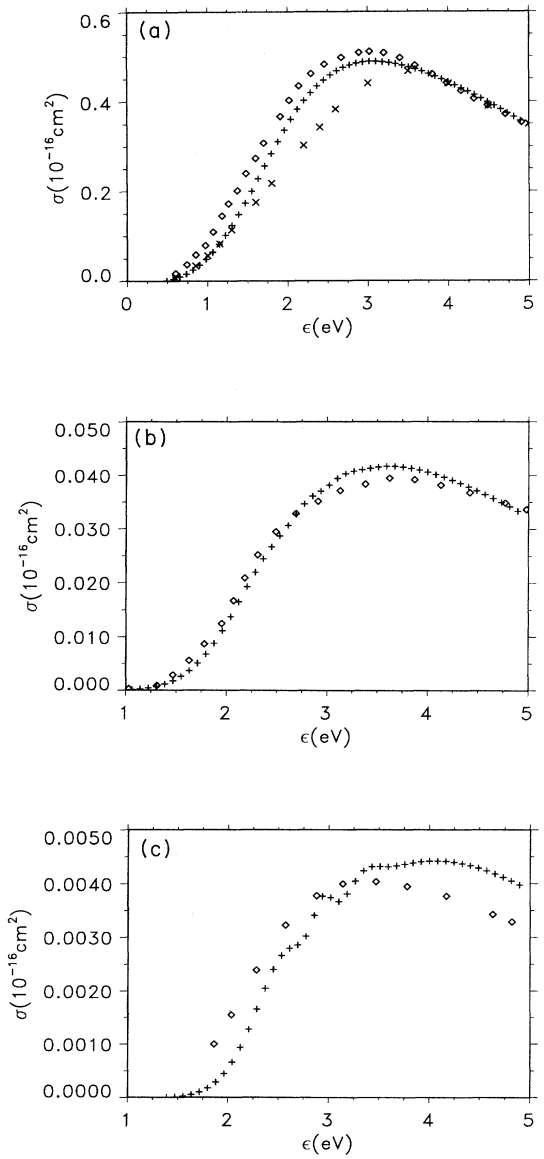

FIG. 5. Vibrational excitation cross sections from experiment (Ref. 1) (◇) and present calculation from the $^2\Sigma_u^+$ symmetry (+): (a) $v = 0 \rightarrow v = 1$; (b) $v = 0 \rightarrow v = 2$; and (c) $v = 0 \rightarrow v = 3$. The experimental data (×) of Ref. 22(c) is also plotted on Fig. 5(a).

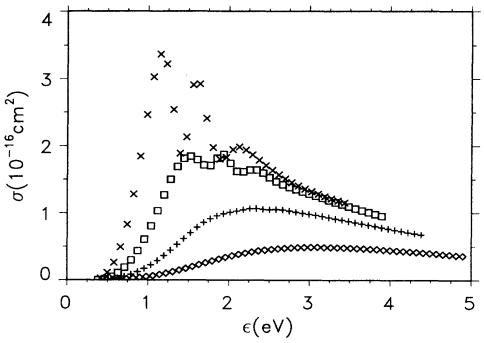

FIG. 6. Present calculation of vibrational excitation cross sections: $v=0\rightarrow v=1$ ($\diamond$), $v=1\rightarrow v=2$ (+), $v=2\rightarrow v=3$ ($\square$), and $v=3\rightarrow v=4$($\times$).

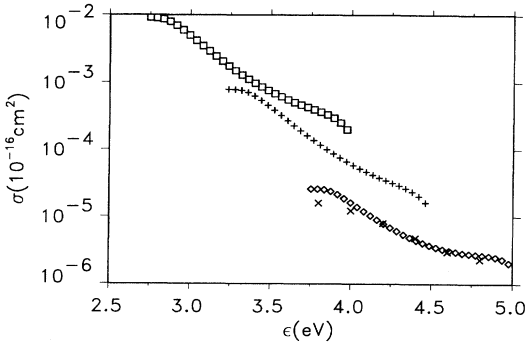

FIG. 7. Present calculation of the dissociative attachment cross sections from the initial vibrational state $v_i=0$ ($\diamond$), $v_i=1$ (+), and $v_i=2$ ($\square$). The experimental data of Ref. 4 for $v_i=0$ are also plotted ($\times$).

the cross sections for vibrational excitation from $v=0$ to $v'=1-3$ and for $\Delta v=1$ from $v_i=0-3$. We did not calculate vibrationally elastic cross sections since much simpler methods do a good job (our results for the elastic channels would be suspect in any case since we ignore the contribution from other partial waves as well as polarization and multipole effects outside of the R-matrix box). Our method does not separate a resonance contribution from a background term[10] rendering this distinction unnecessary, as well as inappropriate, for our purposes.

Figure 5 shows the calculated cross sections (crosses) for the first three vibrational excitation channels in comparison with the experimental data of Ehrhardt *et al.*[1] (diamonds) in the 0–5 eV energy range. The agreement between calculation and experiment is good for all channels. We are also in satisfactory agreement with theory, except on two points. The first point concerns the $v=0\rightarrow v=3$ cross section. Previous calculations obtained results a factor of 2 larger than experiment; the present results are much closer to experiment. The second point concerns the $v=0\rightarrow v=1$ cross section. On Fig. 5(a) we also graph the experimental results of Ref. 22(c). In this range, there is a large difference between experiments carried out by two different methods[23] (beam and swarm[22]). All previous theories matched the beam experiments of Ehrhardt *et al.* usually to a much higher accuracy than claimed in the original experiment. The present results are in better agreement with the beam data (although definitely below previous theories) for energies above ~ 1.5 eV. Below ~ 1.5 eV our results are in better agreement with the swarm data, in contrast to the results of Ref. 23. However, we ignore the S-wave and quadrupole contributions to the cross section, which may be substantial near threshold.

From the initial $v=0$ state, the H_2^- vibrational structure becomes more apparent with increasing Δv, from slight wiggles for $v=0\rightarrow v=2$ to pronounced structure for $v=0\rightarrow v=3$ and higher. This trend was also observed in experiment[24] and previous theory,[10] being explained by the longer resonance lifetime at larger R. These peaks are traced to the elimination of closed channels in our MQDT formulation. The same effect occurs in Fig. 6 which shows the $\Delta v=1$ cross section for initial vibrational states $v_i=0-3$; the increasing magnitude of the cross section with u_i was also expected but cannot be compared with previous theory or experiment.

Figure 7 shows the calculated cross sections for dissociative attachment from $v_i=0-2$. Also shown are the experimental results of Ref. 4. The well-known increase by an order of magnitude from $v_i=0$ to $v_i=1$ and from $v_i=1$ to $v_i=2$ is reproduced. The agreement with experiment of the magnitude and energy dependence of the cross section at threshold is poor. For $v_i=0$, the threshold experimental value[4] usually quoted is 1.6×10^{-21} cm^2 compared to our value of 2.6×10^{-21} cm^2. Previous theories[10,21] yielded results $\geq 3.0\times 10^{-21}$ cm^2. Phenomenological theories[25] yielded dissociative attachment cross sections of $\sim 2.6\times 10^{-21}$ cm^2 The poor agreement with experiment is not difficult to rationalize; the cross section is very small and we expect it to depend sensitively on subtle aspects of the R dependence of fixed-nuclei scattering parameters. It is also possible that the energy width of the electron beam could lower the experimental threshold value.

V. CONCLUSIONS

We have calculated the cross section for vibrational excitation and dissociative attachment in H_2 loosely following the program set out by Greene and Jungen.[6] This *ab initio* study of electron–neutral-species scattering using their method encountered difficulties not addressed in the original treatment based on phenomenological models.[8] However, further refinements[26] may resolve these problems which only affected the larger Δv's; however, we were only able to overcome the anomalies by resorting to a method essentially similar to Ref. 11. The fixed-nuclei phase shifts were derived from a fully *ab initio* R-matrix calculation in prolate spheroidal coordinates (e.g., we did not use a model potential for the exchange interaction). The scattering data were interpolated in E and R by relying on an R-matrix calculation using exact solutions of the full Hamiltonian as basis functions. Without any adjustment of the fixed-nuclei data we obtained cross sections in good agreement with experiment[1–3] for $v=0\rightarrow v=1$ and $v=0\rightarrow v=2$ and good agreement in

magnitude with $v=0\rightarrow v=3$. The dissociative attachment cross section was larger than the usually accepted experimental values[4] by 60% but close to previous *ab initio* calculations.[10] A large discrepancy with experiment may be caused by sensitivity of the calculation to details of the fixed-nuclei scattering parameters or to experimental uncertainties. The H_2^- vibrational structure becomes evident for the larger initial vibrational states of H_2 as well as for the larger Δv's confirming previous theory[10] and experiment.[24]

ACKNOWLEDGMENTS

This work owes much to discussions with U. Fano. His assistance with the manuscript and his support have proven invaluable. I also thank Chris Greene for sharing his expertise and suggesting the method discussed in Sec. III B. This research was supported by National Science Foundation Grant Nos. PHY86-10129 and PHY89-18304.

APPENDIX: CONVERTING THE VARIATIONAL *R* MATRIX TO WIGNER-EISENBUD FORM

In this paper, we have used a further simplification of the variational R-matrix calculation popularized by Greene.[17] This simplification recasts Greene's more powerful variational principle into Wigner-Eisenbud form[27] without loss of flexibility and power, thus combining the best aspects of both methods. The improvement in computing speed over the streamlined form[17(c)] of the R matrix is negligible, but from a pedagogical basis seemed worthy of note. In this formulation, $(\partial\Psi_B/\partial n)+mb_\beta\Psi_\beta=0$ on a closed surface S. The wave function is represented by a superposition of basis functions with alternative logarithmic derivatives on S, $\Psi_\beta=\sum_k y_k(\mathbf{r})c_{k\beta}$, inserted into the variational principle for the b_β, Eq. (4). The best results seem to be obtained when all but two of the trial functions in each channel have the same logarithmic derivative with the logarithmic derivative of the two extra being quite different from the majority (e.g., $n-2$ of the basis functions have zero derivative on the boundary with the other two equaling zero on the boundary). The $c_{k\beta}$'s are extremized to give a generalized eigensystem

$$\sum_l \Gamma_{kl}c_{l\beta}=b_\beta\sum_l \Lambda_{kl}c_{l\beta}\ , \tag{A1}$$

where

$$\Gamma_{kl}=2\int_V dV\, y_k(E-H)y_l-\int_S dS\, y_k\frac{1}{m}\frac{\partial y_l}{\partial n}$$
$$\equiv 2(EO_{kl}-\bar{H}_{kl}) \tag{A2}$$

and

$$\Lambda_{kl}=\int_S dS\, y_k y_l\ . \tag{A3}$$

$\mathbf{O}$ is the overlap matrix and $\bar{\mathbf{H}}$ is the Hamiltonian plus Bloch operator. The $c_{k\beta}$'s are normalized to $\sum_{k,l}\Lambda_{kl}c_{k\beta}c_{l\alpha}=\delta_{\beta\alpha}$. We now recast Λ expanding the basis functions at the surface in a set of real, orthonormal surface harmonics,[17(b)] ϕ_i, $y_{ik}\equiv\int_S dS\,\phi_i y_k$;

$$\Lambda_{kl}=\sum_i y_{ik}y_{il}\ . \tag{A4}$$

Division of Eq. (A1) by Γ and b transforms it into

$$\sum_l y_{il}c_{l\beta}\frac{1}{b_\beta}=\sum_{l,k,j,m}[y_{il}(\Gamma^{-1})_{lk}y_{jk}](y_{jm}c_{m\beta})\ . \tag{A5}$$

Notice that $U_{i\beta}\equiv\sum_l y_{il}c_{l\beta}$ is a unitary matrix and consequently

$$\sum_\beta U_{i\beta}\frac{1}{b_\beta}U_{j\beta}=\sum_{l,k} y_{il}(\Gamma^{-1})_{lk}y_{jk}=R_{ij}\ . \tag{A6}$$

Although we have made a slight conceptual advance from Eq. (A1), in practice Eq. (A6) would be just a difficult to solve as (A1) if not more so, since Γ needs to be manipulated into a form that is easy to invert.

In the final step, the $\bar{H}$ matrix is diagonalized by solving

$$\sum_l \bar{H}_{kl}W_{l\alpha}=\sum_l O_{kl}W_{l\alpha}\varepsilon_\alpha \tag{A7}$$

and normalizing the $W_{l\alpha}$'s to $\sum_{k,l}O_{kl}W_{k\alpha}W_{l\beta}=\delta_{\alpha\beta}$. The R matrix is now in Wigner-Eisenbud form

$$R_{ij}=\tfrac{1}{2}\sum_\alpha\frac{Y_{i\alpha}Y_{j\alpha}}{E-\varepsilon_\alpha}\ , \tag{A8}$$

where

$$Y_{i\alpha}=\sum_l y_{il}W_{l\alpha}\ . \tag{A9}$$

The ε_α are the variational estimates of the energies of the Hamiltonian with the wave function having zero derivative on the boundary, and the $Y_{i\alpha}$ are variational estimates of the amplitudes of the α wave functions in the ith channel. This derivation provides the connection between two R-matrix methods, showing that the Wigner-Eisenbud form of the R matrix is not limited to using basis functions all of which have zero derivative on the surface. This fact has been recognized by some authors (e.g., Ref. 11), but rarely utilized in practical calculations.

*Present address: Joint Institute for Laboratory Astrophysics, Boulder, CO 80309-0440.

[1]H. Ehrhardt, L. Langhans, F. Linder, and H. S. Taylor, Phys. Rev. **173**, 222 (1968).

[2]G. J. Schulz, Rev. Mod. Phys. **45**, 423 (1973).

[3]S. Trajmar, D. F. Register, and A. Chutjian, Phys. Rep. **97**, 219 (1983); N. Lane, Rev. Mod. Phys. **52**, 29 (1980); M. A. Morrison, R. W. Crompton, B. C. Saha, and Z. Lj. Petrovic, Aust. J. Phys. **40**, 239 (1987).

[4]G. J. Schulz and R. K. Asundi, Phys. Rev. Lett. **15**, 946 (1965); Phys. Rev. **158**, 25 (1967).

[5]J. N. Bardsley, A. Herzenberg, and F. Mandl, Proc. Phys. Soc. London **89**, 305 (1966); **89**, 321 (1966).

[6](a) C. H. Greene and Ch. Jungen, Adv. At. Mol. Phys. **21**, 51

(1985); (b) C. H. Greene, Comments At. Mol. Phys. **23**, 209 (1989); (c) Hong Gao and C. H. Greene, J. Chem. Phys. **91**, 3988 (1989).

[7]L. Dubé and A. Herzenberg, Phys. Rev. A **20**, 194 (1979).

[8]C. H. Greene and Ch. Jungen, Phys. Rev. Lett. **55**, 1066 (1985).

[9]R. K. Nesbet, Comments At. Mol. Phys. **11**, 25 (1981).

[10]C. Mündel, M. Berman, and W. Domcke, Phys. Rev. A **32**, 181 (1985); W. Domcke, C. Mündel, and L. S. Cederbaum, Comments At. Mol. Phys. **20**, 293 (1987).

[11]B. I. Schneider, M. Le Dourneuf, and Vo Ky Lan, Phys. Rev. Lett. **43**, 1926 (1979); B. I. Schneider, M. Le Dourneuf, and P. G. Burke, J. Phys. B **12**, L365 (1979).

[12]S. Ross and Ch. Jungen, Phys. Rev. Lett. **59**, 1297 (1987) and Ref. 6(a).

[13]M. J. Seaton, Rep. Prog. Phys. **46**, 167 (1983); C. H. Greene, U. Fano, and G. Strinati, Phys. Rev. A **19**, 1485 (1978).

[14]*Handbook of Mathematical Functions,* edited by M. Abramowitz and I. A. Stegun (Dover, New York, 1972), Chap. 21.

[15](a) S. Hara, J. Phys. Soc. Jpn. **27**, 1009 (1969); (b) B. I. Schneider, Phys. Rev. A **11**, 1957 (1975); (c) B. R. Judd, *Angular Momentum Theory for Diatomic Molecules* (Academic, New York, 1975), Chap. 4.

[16]W. Kołos and L. Wolniewicz, J. Chem. Phys. **43**, 2429 (1965); J. Mol. Spectrosc. **54**, 303 (1975).

[17](a) C. H. Greene, Phys. Rev. A **28**, 2209 (1983); (b) C. H. Greene, in *Fundamental Processes of Atomic Dynamics,* edited by J. S. Briggs, K. Kleinpoppen, and H. O. Lutz (Plenum, New York, 1988), p. 105; (c) C. H. Greene and Longhuan Kim, Phys. Rev. A **38**, 5953 (1988).

[18]A. Klonover and U. Kaldor, J. Phys. B **12**, L61 (1979); **12**, 323 (1979).

[19]J. Senekowitsch, P. Rosmus, W. Domcke, and H. J. Werner, Chem. Phys. Lett. **111**, 211 (1984).

[20]T. L. Gibson and M. A. Morrison, Phys. Rev. A **29**, 2497 (1984).

[21]J. M. Launay and M. Le Dourneuf, in *Electronic and Atomic Collisions: Invited Papers of the XIII International Conference on the Physics of Electronic and Atomic Collisions,* edited by J. Eichler, I. V. Hertel, and N. Stolterfoht (Elsevier, New York, 1984), p. 635.

[22](a) R. W. Crompton, M. T. Elford, and A. G. Robertson, Aust. J. Phys. **23**, 667 (1970); (b) H. B. Milloy and R. W. Crompton, Phys. Rev. A **15**, 1847 (1977); (c) J. P. England, M. T. Elford, and R. W. Crompton, Aust. J. Phys. **41**, 573 (1988).

[23]S. J. Buckman *et al.,* Phys. Rev. Lett. **65**, 3253 (1990).

[24]M. Allan, J. Phys. B **18**, L451 (1985).

[25](a) J. M. Wadehra and J. N. Bardsley, Phys. Rev. Lett. **41**, 1795 (1978); (b) J. Gauyacq, J. Phys. B **18**, 1859 (1985).

[26]Hong Gao and C. H. Greene, Phys. Rev. A **42**, 6946 (1990).

[27]E. P. Wigner and L. Eisenbud, Phys. Rev. **72**, 29 (1947); P. G. Burke and W. D. Robb, Adv. Mol. Phys. **11**, 143 (1975); and Refs. 1–12 of Ref. 17(b).